Editors' Suggestion

High-Efficiency Selective Wireless Power Transfer with a Bistable Parity-Time-Symmetric Circuit

Hongjian Cui,[1,‡] Zhenya Dong,[1,‡] Han-Joon Kim,[1] Chenhui Li,[1] Weijin Chen,[1] Guoqiang Xu,[1] Cheng-Wei Qiu,[1,*] and John S. Ho[1,2,3,†]

[1] *Department of Electrical and Computer Engineering, National University of Singapore, 117583, Singapore*
[2] *Institute for Health Innovation and Technology, National University of Singapore, 117599, Singapore*
[3] *The N.1 Institute for Health, National University of Singapore, 117456, Singapore*

(Received 14 June 2022; revised 16 September 2022; accepted 19 September 2022; published 31 October 2022)

Wireless power transfer from a single transmitter to multiple receivers has broad applications in consumer devices and industrial systems. However, current approaches for achieving selective wireless power transfer among multiple receivers rely on complex tuning schemes, which suffer from reduced efficiency when there are slight deviations from the optimal operating point. Here, we generalize prior analyses of *PT*-symmetric wireless power transfer to the case of multiple receivers and show that the asymmetrical energy distribution arising from operation in a bistable region can solve such problems. Using a system with three equally distant receivers, we experimentally demonstrate wireless power transfer to a selected receiver with 65% efficiency and 99% selectivity without any tuning of the transmitter, achieving localization of 83% of the total energy at the target.

DOI: 10.1103/PhysRevApplied.18.044076

I. INTRODUCTION

Wireless power transfer (WPT) has experienced a resurgence of interest over the past decade with the rise of electronic products such as mobile devices, electric vehicles, and healthcare sensors [1,2]. Among various types of WPT systems, selective WPT from a single transmitter to multiple receivers is of particular scientific and commercial interest because it can enable simultaneous charging of many devices [3–9]. Various approaches have been demonstrated for selective WPT, such as using transmitter arrays to localize a magnetic field at a target receiver or adjusting the frequency of the input signal to match the resonant frequency of the target [10–12]. While these approaches can effectively suppress electromagnetic interactions with devices not in use, the need for external feedback and control mechanisms increases the complexity of circuit implementation [2,8,9,13–19]. Furthermore, because the optimal circuit configuration depends on the coupling strengths between the transmitter and the receivers [1,3], these systems suffer from reduced efficiency and selectivity when there are slight deviations in the operation conditions, which must be compensated by active tuning of the system.

Recently, the concept of parity-time (*PT*) symmetry has gained significant interest as a way to realize robust WPT systems [20–25]. *PT* symmetry describes systems that are invariant under joint parity and time reversal operations [26,27]. The existence of an exceptional point in the eigenfrequency spectrum of the system separates the response into phases in which *PT* symmetry is unbroken and then spontaneously broken, which can lead to unprecedented phenomena in a variety of physical systems [28–31]. In electronics, *PT*-symmetric circuits can be implemented by incorporating a gain element in the transmitter to serve as the time-reversed counterpart to the loss in the receiver [32–36]. When combined with nonlinear gain saturation, such a circuit oscillates naturally at one of its eigenfrequencies without an external driving signal, allowing it to automatically track an optimal operating point across a wide range of system parameters [28,37,38]. Previous works have demonstrated strongly coupled *PT*-symmetric circuits that provide WPT with nearly constant efficiency in the presence of variations in the distance between the transmitter and receiver [20,21,39]. However, the generalization of *PT*-symmetric WPT to systems with multiple receivers and the development of a mechanism to achieve selectivity among the receivers have yet to be demonstrated.

In this paper, we show that bistability in the mode selection dynamics of a nonlinear *PT*-symmetric circuit can be exploited to realize selective WPT with high efficiency. We demonstrate that the bistability provides access to

*chengwei.qiu@nus.edu.sg
†johnho@nus.edu.sg
‡These authors contributed equally to this paper.

eigenmodes in which energy is asymmetrically localized in a subset of receivers detuned from the initial oscillation frequency of the system, leading to suppression of losses in both the transmitter and the remaining receivers. Using a system with three receivers, we experimentally implement a WPT system with transfer efficiency of 65% to the target receiver and selectivity of 99% among other receivers.

II. THEORY

A. Enhanced wireless power transfer in bistable *PT*-symmetric circuit

To understand how bistability enables high-efficiency selective WPT, we first analyze a two-level *PT*-symmetric circuit. Figure 1 shows a comparison between conventional magnet resonant power transfer circuits and bistable WPT. In the conventional WPT system shown in Fig. 1(a), frequency tuning of either the transmitter or receiver resonator is needed to reach a maximum WPT efficiency [2,40]. In contrast, we demonstrate that the power transfer in a bistable circuit avoids such a requirement. To achieve a bistable circuit, the source at the transmitter is replaced by a nonlinear saturable gain element as demonstrated in Fig. 1(b). As previously demonstrated in Refs. [20,39], energy injected by the gain element enables the circuit to self-oscillate and—despite the existence of more than one possible mode—settle at a single frequency ω through a mode selection process.

To describe the bistable WPT circuit with coupled mode theory, the self-resonant frequency is set to be ω_1 and net gain rate from single transmitter is g_{net}. The gain at the transmitter g_{net} is equal to $g_1 - \gamma_{10}$, where g_1 is the equivalent gain rate at the amplifier and γ_{10} is the intrinsic loss rate at the load. The self-resonant frequency is ω_j and the loss rate is γ_j at receiver j, where $\gamma_j = \gamma_{jL} + \gamma_{j0}$. γ_{jL} is the loss at load and γ_{j0} is the intrinsic loss at receiver. $\kappa_{1j} = \omega k_{1j}/2$ is the coupling rate between the transmitter and receiver j. For a WPT model with one receiver, the dynamics can be described as [41–43]

$$\begin{pmatrix} \dot{a_1} \\ \dot{a_2} \end{pmatrix} = \begin{pmatrix} i\omega_1 + g_{\text{net}} & -i\kappa_{12} \\ -i\kappa_{12} & i\omega_2 - \gamma_2 \end{pmatrix} \begin{pmatrix} a_1 \\ a_2 \end{pmatrix}, \tag{1}$$

where a_j is normalized oscillation amplitude at transmitter or receiver j, such that $|a_j|^2$ is the stored energy, and $\dot{a}_j$ is the time derivative of a_j.

Note that $\gamma_{10}|a_1|^2$ is the power dissipated in the transmitter and $\gamma_2|a_2|^2$ is the power dissipated in the receiver. The WPT efficiency in the steady state can be expressed as [20]

$$\eta = \frac{\gamma_{2L}}{\gamma_2 + \gamma_{10}(1/\beta - 1)}, \tag{2}$$

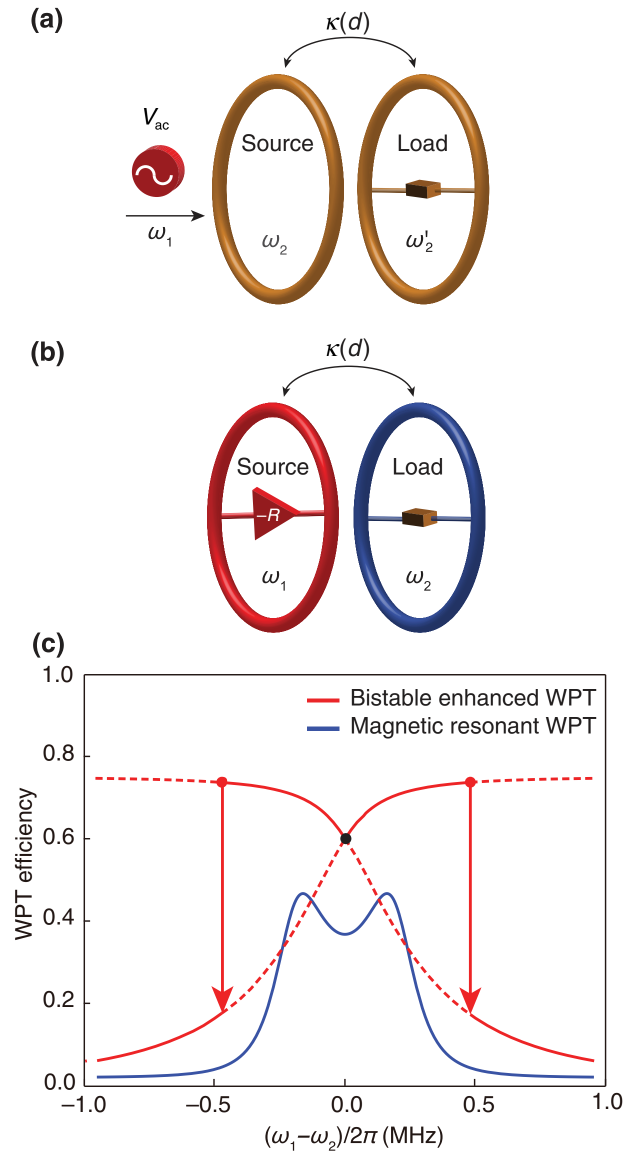

FIG. 1. Comparison between conventional and bistable WPT circuits. (a) Conventional schematic. The source wave with frequency ω_1 is generated and connected to the source coil with resonant frequency of ω_2; the load coil with self-resonant frequency of ω_2' is coupled to the source coil with coupling rate $\kappa(d)$. (b) *PT*-symmetric scheme. Power is generated at the source coil with resonant frequency ω_1; the receiver with resonant frequency ω_2 is coupled to the source coil with coupling rate $\kappa(d)$. (c) Efficiency with detuning of $\omega_2 - \omega_1$. The blue curve indicates a conventional scheme with $\omega_2 = \omega_2'$, while the red curve indicates the *PT*-symmetric scheme. The black dot indicates the working condition in other *PT*-symmetric WPT circuits. The arrow indicates that the WPT efficiency drops with mode switching at the boundary of the bistable region. The receiver and load are perfectly matched.

where $\beta = |a_2|^2/(|a_1|^2 + |a_2|^2)$ is the fraction of energy localized in the receiver. Equation (2) indicates that localization of energy in the receiver ($\beta \to 1$) provides enhanced efficiency.

Here, we show that a high value of β can be obtained with large frequency detuning $|\omega_1 - \omega_2|$ at the boundary of the bistable region. To reach the bistable region, strong coupling where $\kappa_{12} > (\gamma_2 + g_{\text{net}})/2$ should be satisfied. The eigenfrequencies that represent modes of the system can be derived from Eq. (1). With the strong coupling condition, two real eigenfrequencies ω_+ and ω_- representing two modes coexist.

The energy distribution β can be obtained by calculating the corresponding eigenvectors a_1 and a_2 at the two eigenmodes $\omega_\pm$, which are the relative oscillation amplitudes of the transmitter and receiver:

$$\frac{a_{1\pm}}{a_{2\pm}} = -\frac{-i\gamma_2 - ig_{\text{net}} + \omega_1 - \omega_2}{2\kappa_{12}} \mp \frac{\sqrt{4\kappa_{12}^2 - [\gamma_2 + g_{\text{net}} + i(\omega_1 - \omega_2)]^2}}{2\kappa_{12}}. \quad (3)$$

To show how the WPT efficiency changes with detuning in such a system, ω_1 and coupling rate κ_{12} are initially fixed. By gradually tuning the self-resonant frequency ω_2 at the receiver, β can be obtained. Figure 1(c) shows the the calculated efficiency as a function of the detuning $\omega_1 - \omega_2$. The system satisfies PT symmetry when the resonant frequencies are matched $\omega_1 = \omega_2$ such that the amplitude distribution is equal, $\beta = 0.5$. Remarkably, bistability allows the system to access a region where the amplitude at the receiver exceeds that of the transmitter, $\beta > 0.5$, resulting in even higher efficiency. When the detuning $\omega_1 - \omega_2$ goes beyond this region, the system spontaneously switches to a different mode where $\beta < 0.5$, resulting in low transfer efficiency.

The degree to which energy can be localized in the target receiver is limited by the width of the bistable region. Assuming that g_1 can be arbitrarily large, the boundaries of the bistable region are given by

$$\omega_{2,\pm} = \omega_1 \pm \frac{\sqrt{\kappa_{12}(8\gamma_2^2 + \kappa_{12}^2)^{3/2} - 20\gamma_2^2\kappa_{12}^2 - 8\gamma_2^4 + \kappa_{12}^4}}{4\gamma_2/\sqrt{2}}, \quad (4)$$

where $\omega_{2,+}$ is the upper bound and $\omega_{2,-}$ is the lower bound on ω_2. Such behavior persists in systems with multiple receivers ($n > 2$) as described in the next section.

B. Selective wireless power transfer with multiple receivers

In the multireceiver WPT model, bistable behavior still exists and can lead to high-efficiency selective WPT. A schematic of the system is shown in Fig. 2(a). With the same parameters as in Eq. (1), the dynamics of the system can be described as

$$\begin{pmatrix} \dot{a}_1 \\ \dot{a}_2 \\ \vdots \\ \dot{a}_n \end{pmatrix} = \begin{pmatrix} i\omega_1 + g_{\text{net}} & -i\kappa_{12} & \cdots & -i\kappa_{1n} \\ -i\kappa_{12} & i\omega_2 - \gamma_2 & \cdots & 0 \\ \vdots & \vdots & \ddots & 0 \\ -i\kappa_{1n} & 0 & \ldots & i\omega_n - \gamma_n \end{pmatrix} \begin{pmatrix} a_1 \\ a_2 \\ \vdots \\ a_n \end{pmatrix}. \quad (5)$$

For simplicity, there is no coupling between each receiver. The WPT efficiency to the selected receiver associated with resonator 2 is

$$\eta_2 = \frac{\gamma_{2L}}{\gamma_2(1/\beta - 1/\alpha) + \gamma_{10}/\alpha}, \quad (6)$$

where $\beta = |a_2|^2/(|a_1|^2 + \sum_{j=2}^{4} |a_j|^2)$ is the fraction of energy in the target receiver and $\alpha = |a_2|^2/|a_1|^2$ is the ratio of energy in the target receiver to that in the transmitter. High efficiency can be achieved in the bistable region with $\beta \to 1$ when the selected receiver's resonant frequency is tuned.

Analysis is done by setting all the self-resonant frequencies and coupling coefficients between transmitter and each receiver to be equal initially. Then we tune the selected receiver with self-resonant frequency ω_2. The behavior of the system can be visualized by initially setting the parameters $\omega_1/(2\pi) = \omega_3/(2\pi) = \cdots = \omega_n/(2\pi) = 1$ MHz, $g_1 = 1.592 \times 10^5$ s^{-1}, $\kappa_{1j} = 1.5 \times 10^5$ s^{-1}, $\gamma_{10} = 3.98 \times 10^3$ s^{-1}, $\gamma_j = 1.592 \times 10^4$ s^{-1}, and $\gamma_{jL} = 1.194 \times 10^4$ s^{-1}. Thus strong coupling is satisfied as $\kappa_{1j} = \kappa_{12} > (g_1 - \gamma_{10} + \gamma_2)/(2\sqrt{(n-1)})$. By gradual tuning of the selected resonator's resonant frequency ω_2, the evolution of the system's real eigenfrequencies $\text{Re}(\omega)$ representing different modes can be depicted as in Fig. 2(b). For the single-receiver model when $n = 2$, two eigenmodes $\omega_\pm$ that track the tuning frequency ω_2 are presented. For higher-level system with multiple receivers, where $n > 2$, new modes that are insensitive to ω_2 are introduced. The mode with eigenfrequencies $\omega_\pm$ close to ω_2 corresponds to the bistable mode where high-efficiency selective WPT happens.

To explain why the bistable mode suppresses the other modes in the multireceiver system, Fig. 2(c) plots corresponding growth rates of different modes, $-\text{Im}(\omega)$. Growing modes $-\text{Im}(\omega) > 0$ compete to access the gain while the decaying modes $-\text{Im}(\omega) < 0$ vanish in the steady state [20,44]. According to Fig. 2(c), with sweeping of ω_2, the highest growth rates are dominated by mode $\omega_\pm$, which indicates that the system will self-oscillate at one of these frequencies. In contrast, the remaining modes either are decaying or have lower growth rates. Thus, these modes are not selected by mode competition.

When the system is initialized with $\omega_2 > \omega_1$, the gain rate at eigenfrequency ω_- is the highest, and therefore

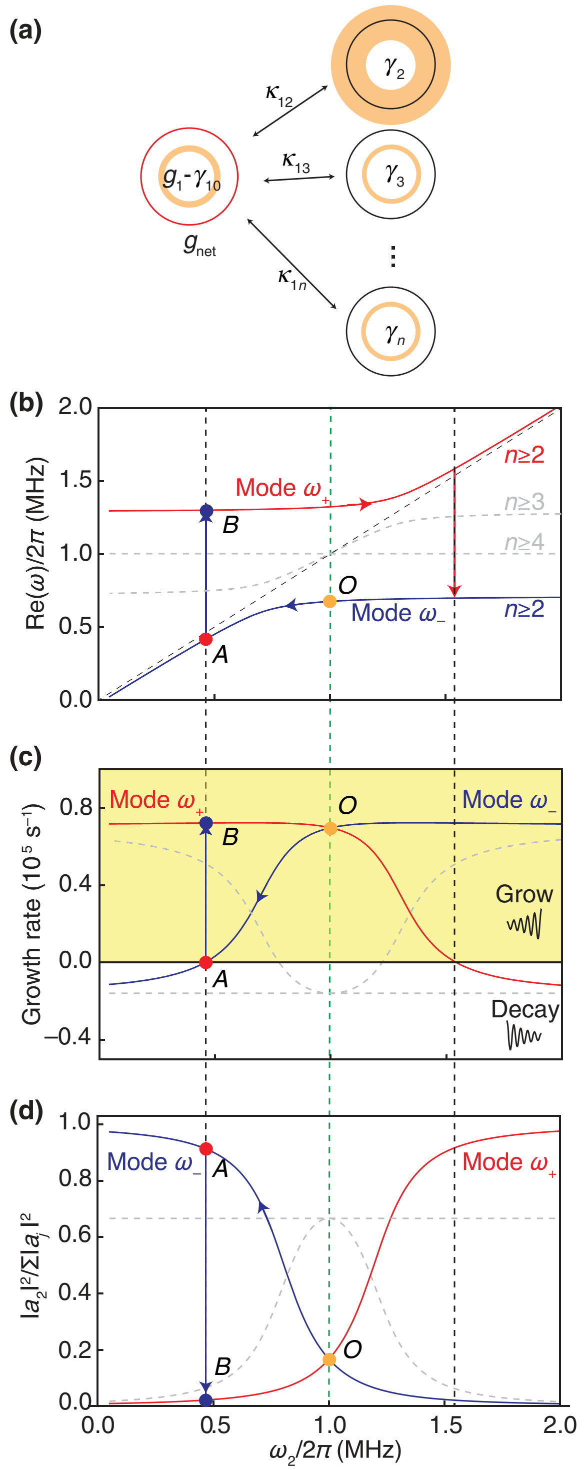

FIG. 2. Analysis of bistable multireceiver WPT system. (a) Setup of selective WPT. (b) Real part of eigenfrequencies. Red and blue lines are modes when $n = 2$, dashed gray lines are modes introduced when a second or third receiver is presented. (c) Growth rate $-\mathrm{Im}(\omega)$. (d) Fraction of energy distributed on the selected receiver.

the mode with eigenfrequency ω_- is selected as the oscillation frequency [37,44]. As ω_2 gradually decreases, the region where $\omega_2 < \omega_1$ is then reached. Adiabaticity causes the system to continue to oscillate at ω_- even though the growth rate of ω_+ is larger [45,46]. This region corresponds to selective WPT as ω_- closely tracks ω_2. However, beyond a certain threshold, the growth rate of the mode with eigenfrequency ω_- becomes negative, and the system nonadiabatically transitions to ω_+, which is the mode with the highest growth rate. Figure 2(d) shows evolution of energy localized at selected receiver β with tuning of ω_2. It is observed that a high selectivity can be obtained with large detuning $\epsilon = \omega_2 - \omega_1$ at the boundary of the bistable region.

Figure 3(a) shows the electronic setup for the selective WPT system. As shown in this figure, the gain element is achieved by the negative impedance converter by connecting R_n, R_a, and R_b to the amplifier. Here we further evaluate the energy distribution behavior with tuning of ω_2 by simulation of magnetic field in Fig. 3(b). With the initial setup when $\omega_2 = \omega_1$ at state O as described in Fig. 2(b), the energy distributed in all the receivers is equal, and the total energy in the receivers is the same as the energy in the transmitter ($\beta = 0.167$ and $\alpha = 0.333$), as depicted in the left-hand panel of Fig. 3(b). With tuning of ω_2, β and α will continue to increase until the system reaches the boundary of the bistable region, point A, where ω_2 is 0.52 MHz. This state as shown in the center panel of Fig. 3(b) has the highest selectivity ($\beta = 0.89$ and $\alpha = 9.64$) with $\eta_2 = 0.72$. Upon leaving the bistable region, the system undergoes an abrupt transition to the state shown in the right-hand panel of Fig. 3(b) where the efficiency of WPT to the selected receiver suddenly drops to $\eta_2 = 0.03$.

Figure 3(c) shows the bistable region as a function of κ_{1j} and the corresponding transfer efficiency to the selected receiver. These results show that the width of the bistable region increases with κ_{1j} and that the transfer efficiency to the selected receiver is highest at the boundaries of the region.

III. EXPERIMENTAL RESULTS

We experimentally demonstrate selective WPT using a system of three receivers. The coils are designed by using copper wire (1 mm in diameter) wrapped around a 3D-printed, acrylonitrile butadiene styrene (ABS)-plastic support. We modify the setup used to characterize bistability by using a five-turn transmitter coil with dimensions $60 \times 10 \times 5$ cm, which has a measured inductance of 23.7 μH. The receiver coils are wrapped with dimensions of $20 \times 10 \times 5$ cm. The gain element is achieved by an operational amplifier (LM6171, Texas Instruments) in negative impedance converter configuration with resistances $R_a = R_b = R_n = 67$ Ω, resulting in a small-signal negative resistance of -67 Ω. The receiver coil is terminated with resistive load of 3300 Ω in parallel with series variable capacitors (GZN60100, Sprague Goodman Electronics) with range given in Table I. With such inductance

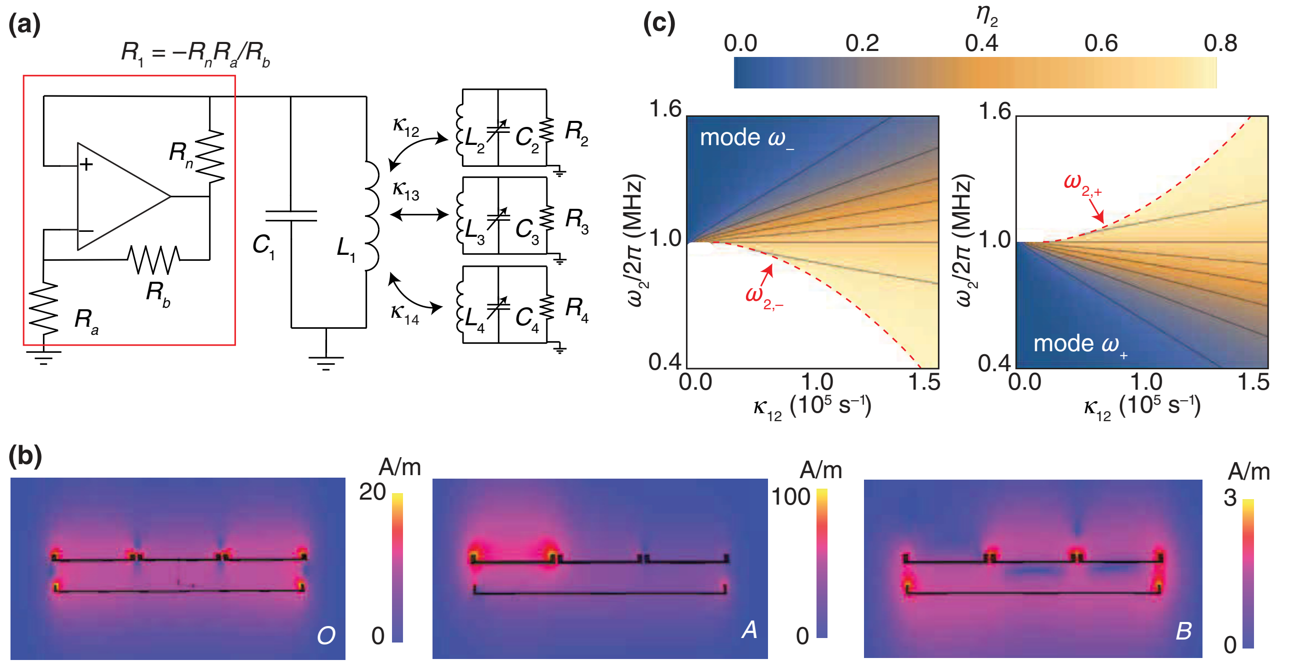

FIG. 3. Circuit setup and simulations. (a) Circuit setup for selective WPT. (b) Plots of magnetic field distribution for the PT-symmetric and detuned configurations. (c) Efficiency of selective WPT η_2 as a function of κ_{1j} and ω_2.

and capacitance, the resonant frequency of the transmitter is initially fixed to be $\omega_1/(2\pi) = 1.01$ MHz.

The receivers are placed at a distance of 3 cm from the transmitter using a foam separator as shown in Fig. 4(a). To achieve selective WPT, we initialize the system such that all of the receivers have the same resonant frequency $\omega_j/(2\pi) = 1.28$ MHz. We then decrease ω_2 by increasing the value of C_2, steering the system to oscillate along the lower bistable branch ω_- to localize the energy at selected tuning receiver.

The system's oscillation frequencies with tuning of ω_2 are shown in Fig. 4(b), measured by using an oscilloscope (Picoscope 6402D, Pico Technology) and extracting the peak of the fast Fourier transform spectrum. When $\omega_2/(2\pi)$ is decreased from 1.28 to 0.643 MHz, the oscillation frequency of the system $\omega_-/(2\pi)$ gradually tracks $\omega_2/(2\pi)$, decreasing from 0.923 to 0.6397 MHz. With continuing tuning when $\omega_2/(2\pi)$ is smaller than 0.643 MHz, the system exits the bistable region. Thus, a sudden system oscillation frequency shift from 0.6397 to 1.04 MHz is observed as described in the theory, representing the system mode shifting.

TABLE I. Circuit parameters for selective WPT.

Parameters	Values
R_a, R_b, R_n	67 Ω
R_2, R_3, R_4	3300 Ω
L_1	23.7 μH
L_2, L_3, L_4	23.9 μH
C_1	0.5 nF
C_2	0.65–2.6 nF

The evolution of the voltages in the transmitter and receivers, and the efficiency of power transfer to each receiver, are shown in Fig. 4(c). The time-averaged power delivered to the load is directly calculated as $P_{2L,\text{ave}} = V_{2,\text{rms}}^2/R_2$, with $V_{2,\text{rms}}$ being the root mean square of the voltage, while the time-averaged power dissipated in the transmitter is obtained by integrating the product of the instantaneous voltage and current, obtained using a current probe (CT1, Tektronix), over one cycle. Initially, the system is at the mode indicated as point O where all receivers have the same self-resonant frequency. The voltage in the transmitter at this state is $V_{1,\text{rms}} = 9.582$ V, and the voltage in each receiver is measured as $V_{j,\text{rms}} = 3.06$ V. However, as $\omega_2/(2\pi)$ is decreased from 1.28 to 0.643 MHz, the voltage in the target receiver $V_{2,\text{rms}}$ increases while the voltage in the transmitter $V_{1,\text{rms}}$ and the other receivers is suppressed. At the boundary of the bistable region, $V_{2,\text{rms}}$ is about 18 V and hence twice $V_{1,\text{rms}}$ and 13 times higher than the voltage in the other receivers. This state corresponds to a transfer efficiency of 65% to the target receiver, which is 6.2 times higher than the initial state. The selectivity of power transfer, defined as the ratio of power delivered to the target receiver to the power delivered to all of the receivers, is 99% with 80% of the total power being delivered to the target receiver. When the tuning shifts the

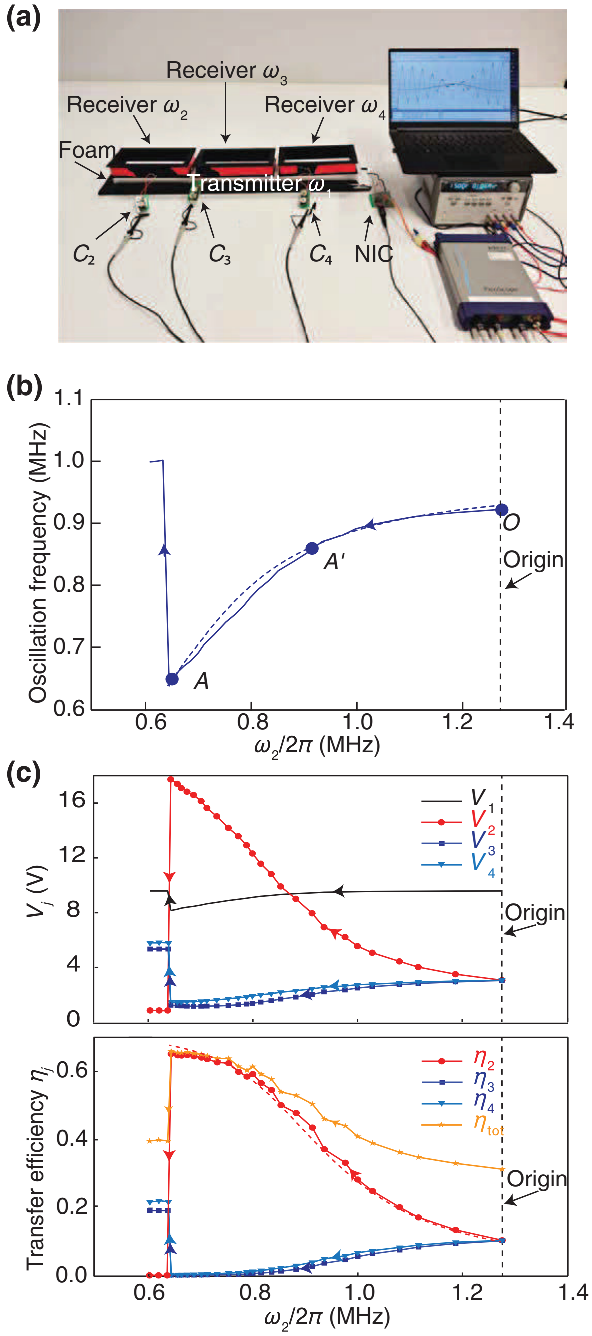

FIG. 4. Experimental setup and results. (a) Image of the setup for selective WPT. (b) System oscillation frequencies as a function of ω_2. Solid blue line shows the experimentally measured frequency and dashed blue line the theoretically predicted eigenfrequencies. (c) Experimentally measured voltage and transfer efficiency at the jth resonator as ω_2 is decreased. Dashed red line shows the theoretically predicted transfer efficiency η_2 to the target receiver.

operating point outside of the bistable region, the voltage in the target receiver drops below 1 V while the voltage at the transmitter is at 9 V, resulting in a WPT efficiency to the selected receiver $\eta_2 < 1\%$.

IV. CONCLUSION

We theoretically and experimentally demonstrate efficient and selective WPT using bistability in a self-oscillating system. The bistability allows the system's oscillation to track the resonant frequency of a strongly coupled receiver as it is detuned from the rest of the system, enabling energy to be selectively localized at the target while suppressing dissipation elsewhere. We successfully achieve an efficient WPT system that does not require any active frequency tuning and also circumvents impedance matching issues.

Future work will be needed to address the potential sensitivity of the system to variations in the operating conditions. Because the scheme requires operating near the boundaries of the bistable region, a small decrease in the coupling strength may cause the system's oscillation frequency to abruptly transit to a different branch, resulting in low transfer efficiency to the target receiver. This sensitivity can be mitigated at the expense of slightly reduced efficiency by limiting the degree of detuning as a function of the coupling strength. Methods to determine the width of the bistable region for more complex configurations may be useful for this task. Furthermore, the design of amplifiers is important to achieve high overall efficiency (including dc-to-ac conversion losses), particularly for high-power systems. In this regard, class-E and switch-mode amplifiers with high-power input have been used to improve the efficiency of high-power WPT systems [39].

ACKNOWLEDGMENTS

This work is supported by grants from the National Research Foundation Singapore (Grant No. NRF-NRFF2017-07) and the Ministry of Education Singapore (No. MOE2016-T3-1-004), and by the Institute for Health Innovation and Technology, National University of Singapore.

APPENDIX: CORRESPONDENCE WITH CIRCUIT ANALYSIS

Consider an inductively coupled single-transmitter, multireceiver parallel *RLC* WPT system. The voltages and currents are related as

$$\begin{pmatrix} V_1 \\ V_2 \\ \vdots \\ V_n \end{pmatrix} = i\omega \begin{pmatrix} L_1 & M_{12} & \cdots & M_{1n} \\ M_{12} & L_2 & \cdots & 0 \\ \vdots & \vdots & \ddots & 0 \\ M_{1n} & 0 & \ldots & L_n \end{pmatrix} \begin{pmatrix} I_{L,1} \\ I_{L,2} \\ \vdots \\ I_{L,n} \end{pmatrix}, \quad \text{(A1)}$$

where M_{1j} is the mutual coupling between transmitter and receiver j and L_j is inductance of coil with number j. V_j is the voltage and $I_{L,j}$ is the current flowing through the inductor L_j. Kirchoff's laws for the WPT circuit with one transmitter and one receiver can be given as

$$
\begin{aligned}
I_{L,1} + \frac{V_1}{R_1} + i\omega C_1 V_1 &= 0,\\
I_{L,2} + \frac{V_2}{R_2} + i\omega C_2 V_2 &= 0,\\
&\vdots\\
I_{L,n} + \frac{V_n}{R_n} + i\omega C_n V_n &= 0,
\end{aligned}
\tag{A2}
$$

where C_j is the capacitance and R_j is the resistance of resonator j. ω is the resonant frequency of the system. Eliminating V_n by combining Eqs. (A1) and (A2), we obtain

$$
\begin{pmatrix}
-i\omega L_1 + \frac{iR_1}{-i+C_1R_1\omega} & -i\omega M_{12} & \cdots & -i\omega M_{1n}\\
-i\omega M_{12} & -i\omega L_2 + \frac{iR_2}{-i+C_2R_2\omega} & \cdots & 0\\
\vdots & \vdots & \ddots & 0\\
-i\omega M_{1n} & 0 & \cdots & -i\omega L_n + \frac{iR_n}{-i+C_nR_n\omega}
\end{pmatrix}
\begin{pmatrix} I_{L,1}\\ I_{L,2}\\ \vdots\\ I_{L,n}\end{pmatrix}
=
\begin{pmatrix} 0\\ 0\\ \vdots\\ 0\end{pmatrix}.
\tag{A3}
$$

To simplify Eq. (A3), the self-resonant frequency and loss of the n-level system of two RLC oscillators are given as $\omega_j = 1/\sqrt{L_j C_j}$ and $\gamma_j = 1/(2R_j C_j)$. The amplitude a_n can be related to the current flowing through the inductor $a_j = I_{L,j}\sqrt{L_j/2}$. $k_{1j} = M_{1j}/\sqrt{L_1 L_j}$ is the coupling coefficient between transmitter and receiver j and $\omega/2\pi$ is the oscillation frequency of the system. Equation (A3) can be thus converted to

$$
\begin{pmatrix}
\frac{-2i\gamma_1\omega+\omega^2-\omega_1^2}{4\gamma_1+2i\omega} & \frac{-ik_{12}\omega}{2} & \cdots & \frac{-ik_{1n}\omega}{2}\\
\frac{-ik_{12}\omega}{2} & \frac{-2i\gamma_2\omega+\omega^2-\omega_2^2}{4\gamma_2+2i\omega} & \cdots & 0\\
\vdots & \vdots & \ddots & 0\\
\frac{-ik_{1n}\omega}{2} & 0 & \cdots & \frac{-2i\gamma_n\omega+\omega^2-\omega_n^2}{4\gamma_n+2i\omega}
\end{pmatrix}
\begin{pmatrix} a_1\\ a_2\\ \vdots\\ a_n\end{pmatrix}
=
\begin{pmatrix} 0\\ 0\\ \vdots\\ 0\end{pmatrix}.
\tag{A4}
$$

For oscillators that are inductively coupled, the coupling rate κ_{1j} between transmitter and receiver j is given by $\kappa_{1j} = \omega M_{1j}/(2\sqrt{L_1 L_j}) = \omega k_{1j}/2$. With the approximation that $k << 1$ and $\gamma_n << \omega_n$, we have $\omega(\omega_n^2 - 1)/2 \approx \omega_n - \omega$. As γ_1 is a gain element, we can replace it with g_{net}. Equation (A4) reduces to

$$
\begin{pmatrix}
i(\omega_1-\omega)+g_{\text{net}} & -i\kappa_{12} & \cdots & -i\kappa_{1n}\\
-i\kappa_{12} & i(\omega_2-\omega)-\gamma_2 & \cdots & 0\\
\vdots & \vdots & \ddots & 0\\
\frac{-ik_{1n}\omega}{2} & 0 & \cdots & -i\kappa_{1n}-\gamma_n
\end{pmatrix}
\begin{pmatrix} a_1\\ a_2\\ \vdots\\ a_n\end{pmatrix}
=
\begin{pmatrix} 0\\ 0\\ \vdots\\ 0\end{pmatrix}.
\tag{A5}
$$

[1] A. Kurs, A. Karalis, R. Moffatt, J. D. Joannopoulos, P. Fisher, and M. Soljačić, Wireless power transfer via strongly coupled magnetic resonances, Sci. **317**, 83 (2007).
[2] A. P. Sample, D. T. Meyer, and J. R. Smith, Analysis, experimental results, and range adaptation of magnetically coupled resonators for wireless power transfer, IEEE Trans. Ind. Electron. **58**, 544 (2010).
[3] B. L. Cannon, J. F. Hoburg, D. D. Stancil, and S. C. Goldstein, Magnetic resonant coupling as a potential means for wireless power transfer to multiple small receivers, IEEE Trans. Power Electron. **24**, 1819 (2009).

[4] Z. N. Low, J. J. Casanova, and J. Lin, A loosely coupled planar wireless power transfer system supporting multiple receivers, Adv. Power Electron. **2010**, 546529 (2010).
[5] D. Ahn and S. Hong, Effect of coupling between multiple transmitters or multiple receivers on wireless power transfer, IEEE Trans. Ind. Electron. **60**, 2602 (2012).
[6] S. Kisseleff, I. F. Akyildiz, and W. H. Gerstacker, Magnetic induction-based simultaneous wireless information and power transfer for single information and multiple power receivers, IEEE Trans. Commun. **65**, 1396 (2016).
[7] M. Fu, H. Yin, M. Liu, Y. Wang, and C. Ma, A 6.78 MHz multiple-receiver wireless power transfer system with constant output voltage and optimum efficiency, IEEE Trans. Power Electron. **33**, 5330 (2017).
[8] Y.-J. Kim, D. Ha, W. J. Chappell, and P. P. Irazoqui, Selective wireless power transfer for smart power distribution in a miniature-sized multiple-receiver system, IEEE Trans. Ind. Electron. **63**, 1853 (2015).
[9] Z. Dai, Z. Fang, H. Huang, Y. He, and J. Wang, Selective omnidirectional magnetic resonant coupling wireless power transfer with multiple-receiver system, IEEE Access **6**, 19287 (2018).
[10] B. H. Waters, B. J. Mahoney, V. Ranganathan, and J. R. Smith, Power delivery and leakage field control using an adaptive phased array wireless power system, IEEE Trans. Power Electron. **30**, 6298 (2015).
[11] K. Sun, R. Fan, X. Zhang, Z. Zhang, Z. Shi, N. Wang, P. Xie, Z. Wang, G. Fan, and H. Liu, *et al.*, An overview of metamaterials and their achievements in wireless power transfer, J. Mater. Chem. C **6**, 2925 (2018).
[12] H. Jung and B. Lee, Optimization of magnetic field focusing and null steering for selective wireless power transfer, IEEE Trans. Power Electron. **35**, 4622 (2019).
[13] Y. Zhang, T. Lu, Z. Zhao, F. He, K. Chen, and L. Yuan, Selective wireless power transfer to multiple loads using receivers of different resonant frequencies, IEEE Trans. Power Electron. **30**, 6001 (2014).
[14] T. Nakagawa, K. Furusato, T. Nozaki, T. Murakami, and T. Imura, in *2017 International Symposium on Antennas and Propagation (ISAP)* (IEEE, 2017), p. 1.
[15] C. Jiang, K. Chau, T. Ching, C. Liu, and W. Han, Time-division multiplexing wireless power transfer for separately excited dc motor drives, IEEE Trans. Mag. **53**, 1 (2017).
[16] K. Lee and S. H. Chae, Comparative analysis of frequency-selective wireless power transfer for multiple-Rx systems, IEEE Trans. Power Electron. **35**, 5122 (2019).
[17] Y. Zhang, Z. Zhao, and K. Chen, Frequency-splitting analysis of four-coil resonant wireless power transfer, IEEE Trans. Ind. Appl. **50**, 2436 (2013).
[18] J. Park, Y. Tak, Y. Kim, Y. Kim, and S. Nam, Investigation of adaptive matching methods for near-field wireless power transfer, IEEE Trans. Ant. Propag. **59**, 1769 (2011).
[19] T. C. Beh, M. Kato, T. Imura, S. Oh, and Y. Hori, Automated impedance matching system for robust wireless power transfer via magnetic resonance coupling, IEEE Trans. Ind. Electron. **60**, 3689 (2012).
[20] S. Assawaworrarit, X. Yu, and S. Fan, Robust wireless power transfer using a nonlinear parity–time-symmetric circuit, Nature **546**, 387 (2017).
[21] M. Sakhdari, M. Hajizadegan, and P.-Y. Chen, Robust extended-range wireless power transfer using a higher-order PT-symmetric platform, Phys. Rev. Res. **2**, 013152 (2020).
[22] C. Zeng, Y. Sun, G. Li, Y. Li, H. Jiang, Y. Yang, and H. Chen, High-Order Parity-Time Symmetric Model for Stable Three-Coil Wireless Power Transfer, Phys. Rev. Appl. **13**, 034054 (2020).
[23] M. Song, P. Jayathurathnage, E. Zanganeh, M. Krasikova, P. Smirnov, P. Belov, P. Kapitanova, C. Simovski, S. Tretyakov, and A. Krasnok, Wireless power transfer based on novel physical concepts, Nat. Electron. **4**, 707 (2021).
[24] J. Song, F. Yang, Z. Guo, X. Wu, K. Zhu, J. Jiang, Y. Sun, Y. Li, H. Jiang, and H. Chen, Wireless Power Transfer via Topological Modes in Dimer Chains, Phys. Rev. Appl. **15**, 014009 (2021).
[25] H. Kim, S. Yoo, H. Joo, J. Lee, D. An, S. Nam, H. Han, D.-H. Kim, and S. Kim, Wide-range robust wireless power transfer using heterogeneously coupled and flippable neutrals in parity-time symmetry, Sci. Adv. **8**, eabo4610 (2022).
[26] C. M. Bender, *PT Symmetry: In Quantum and Classical Physics* (World Scientific, Singapore, 2019).
[27] C. M. Bender, Making sense of non-Hermitian Hamiltonians, Rep. Prog. Phys. **70**, 947 (2007).
[28] X. Shu, A. Li, G. Hu, J. Wang, A. Alù, and L. Chen, Fast encirclement of an exceptional point for highly efficient and compact chiral mode converters, Nat. Commun. **13**, 1 (2022).
[29] S. K. Gupta, Y. Zou, X.-Y. Zhu, M.-H. Lu, L.-J. Zhang, X.-P. Liu, and Y.-F. Chen, Parity-time symmetry in non-Hermitian complex optical media, Adv. Mater. **32**, 1903639 (2020).
[30] S. Kananian, G. Alexopoulos, and A. S. Poon, Coupling-Independent Real-Time Wireless Resistive Sensing through Nonlinear *PT* Symmetry, Phys. Rev. Appl. **14**, 064072 (2020).
[31] B. Zhu, Q. J. Wang, and Y. D. Chong, Laser-mode bifurcations induced by PT-breaking exceptional points, Phys. Rev. A **99**, 033829 (2019).
[32] J. Schindler, A. Li, M. C. Zheng, F. M. Ellis, and T. Kottos, Experimental study of active *LRC* circuits with *PT* symmetries, Phys. Rev. A **84**, 040101 (2011).
[33] J. Schindler, Z. Lin, J. Lee, H. Ramezani, F. M. Ellis, and T. Kottos, PT-symmetric electronics, J. Phys. A: Math. Theor. **45**, 444029 (2012).
[34] P.-Y. Chen, M. Sakhdari, M. Hajizadegan, Q. Cui, M. M.-C. Cheng, R. El-Ganainy, and A. Alù, Generalized parity–time symmetry condition for enhanced sensor telemetry, Nat. Electron. **1**, 297 (2018).
[35] M. Yang, Z. Ye, M. Farhat, and P.-Y. Chen, Ultrarobust wireless interrogation for sensors and transducers: A non-Hermitian telemetry technique, IEEE Trans. Instrum. Meas. **70**, 1 (2021).
[36] K. Yin, Y. Huang, C. Ma, X. Hao, X. Gao, X. Ma, and T. Dong, Wireless real-time capacitance readout based on perturbed nonlinear parity-time symmetry, Appl. Phys. Lett. **120**, 194101 (2022).

[37] Z. Dong, H.-J. Kim, H. Cui, C. Li, C.-W. Qiu, and J. S. Ho, Wireless Magnetic Actuation with a Bistable Parity-Time-Symmetric Circuit, Phys. Rev. Appl. **15**, 024023 (2021).

[38] S. V. Smirnov, M. O. Makarenko, S. V. Suchkov, D. Churkin, and A. A. Sukhorukov, Bistable lasing in parity-time symmetric coupled fiber rings, Photonics Res. **6**, A18 (2018).

[39] S. Assawaworrarit and S. Fan, Robust and efficient wireless power transfer using a switch-mode implementation of a nonlinear parity–time symmetric circuit, Nat. Electron. **3**, 273 (2020).

[40] A. Bodrov and S.-K. Sul, *Analysis of Wireless Power Transfer by Coupled Mode Theory (CMT) and Practical Considerations to Increase Power Transfer Efficiency* (INTECH Open Access Publisher, London, 2012).

[41] J. Zhou, B. Zhang, W. Xiao, D. Qiu, and Y. Chen, Nonlinear parity-time-symmetric model for constant efficiency wireless power transfer: Application to a drone-in-flight wireless charging platform, IEEE Trans. Ind. Electron. **66**, 4097 (2018).

[42] M. Bertolotti, Waves and fields in optoelectronics, Opt. Acta **32**, 748 (1985).

[43] Z. Dong, Z. Li, F. Yang, C.-W. Qiu, and J. S. Ho, Sensitive readout of implantable microsensors using a wireless system locked to an exceptional point, Nat. Electron. **2**, 335 (2019).

[44] H. Wang, S. Assawaworrarit, and S. Fan, Dynamics for encircling an exceptional point in a nonlinear non-Hermitian system, Opt. Lett. **44**, 638 (2019).

[45] J. Doppler, A. A. Mailybaev, J. Böhm, U. Kuhl, A. Girschik, F. Libisch, T. J. Milburn, P. Rabl, N. Moiseyev, and S. Rotter, Dynamically encircling an exceptional point for asymmetric mode switching, Nature **537**, 76 (2016).

[46] A. U. Hassan, B. Zhen, M. Soljačić, M. Khajavikhan, and D. N. Christodoulides, Dynamically Encircling Exceptional Points: Exact Evolution and Polarization State Conversion, Phys. Rev. Lett. **118**, 093002 (2017).